AIAA JOURNAL
Vol. 39, No. 9, September 2001

Turbulence Structures and the Acoustic Far Field of a Mach 1.3 Jet

James Hileman* and Mo Samimy†
The Ohio State University, Columbus, Ohio 43210

The temporal characteristics of the acoustic far field of a Mach 1.3, high-Reynolds-number, ideally expanded axisymmetric jet and their potential correlation with large-scale turbulence structures within the jet were explored. A dual microphone array, placed approximately 30 deg from the jet axis in the acoustic far field, was used to determine the temporal variations of the acoustic field and the approximate locations of intense noise sources within the jet, as well as the time of noise emission with respect to the acquired planar flow images. Simultaneous double-pulse flow visualizations were used to identify turbulence structures, as well as their development and interaction in the region of intense noise generation. The time history of the acoustic data showed individual large-amplitude noise events, periodic large-amplitude noise events, and long periods of relative quiet without any large-amplitude noise production. These three particular noise events were shown to constitute a significant portion of the sound pressure time traces. It is believed that a fundamental understanding of the mechanisms involved in the production of these events could lead to substantial reductions in the turbulent mixing noise caused by large-scale structures. Based on these preliminary results, interactions between and tearing of large-scale structures within the mixing layer were speculated as mechanisms of large-amplitude noise generation.

Nomenclature

D	=	jet exit diameter
d	=	location of noise source measured from nozzle exit
d_{LF}	=	location of noise emitting region during first laser pulse, measured from nozzle exit
f	=	frequency
M_c	=	convective Mach number
Re	=	Reynolds number, $\rho u D/\mu$
Sr_D	=	Strouhal number, fD/u_j
s	=	sideline distance to microphone array
t_L	=	time lag between noise emission and laser illumination
t_m	=	time between laser illumination and peak noise measurement at front microphone
u_c	=	convective velocity of the large-scale structures
u_j	=	jet exit velocity
x_0	=	downstream distance of the front microphone within array
Δx_m	=	space between the two microphones
τ	=	time separation between sound event reaching each microphone
σ	=	standard deviation of the sound pressure data

Introduction

MOST of the previous experimental work in jet noise research has used statistical methods to obtain information on noise sources. These types of techniques have yielded tremendous information regarding the average noise source location, but they have not provided sufficient information about the mechanisms behind noise production. For the most part, the noise emission process has been treated as a black box within the jet mixing layer, and the relation between the turbulence structures in the jet and noise production has not received enough attention. The reasons for this are many, but the main one has been the lack of experimental methods that can make planar or global, temporally resolved qualitative or quantitative measurements within a high-Reynolds-number, high-speed jet and then relate them to the far-field acoustics. The work presented here is the initial part of an ongoing research project that has an ultimate goal of relating the turbulence structures of a high-Reynolds-number, high-speed jet to its far-field noise via flow visualizations with simultaneous acoustic measurements.

The existence and importance of large-scale structures within relatively high Reynolds number, but low-speed, mixing layers have been well known for about 30 years.[1,2] Large eddies have been shown to evolve and interact in three ways.[3] First, structures form and convect downstream entraining fluid from the ambient and grow in size. Second, a fast moving structure will catch up with a slower structure that is downstream. When they approach one another, they begin to rotate about a common point; this leads to pairing of the two structures.[4] Pairing can occur with just a portion of a structure combining with another whole structure, partial pairing, or when parts of two different structures pair to form a new structure, fractional pairing.[5] Third, individual structures have been observed to tear into two or more separate structures.[3] The tearing process typically involves the fast stream fluid tearing away a portion of a structure contained in the mixing layer.

A large-scale structure within the jet shear layer has an average convective velocity u_c and a convective Mach number M_c (Refs. 6 and 7). The convective velocity is important in aeroacoustics, in general, and in this study, in particular, because it will be used to determine the location of noise emitting regions during flow visualization. The theoretical equation for the convective velocity of the large-scale structure is given by

$$u_c = a_0 u_j/(a_0 + a_j) \tag{1}$$

where u_j and a_j are the jet centerline velocity and speed of sound, respectively, and a_0 is the ambient speed of sound. Similarly, the theoretical convective Mach number is given by

$$M_c = u_j/(a_0 + a_j) \tag{2}$$

The equation for the convective velocity has been shown to be accurate for convective Mach numbers up to approximately 0.5. As the convective Mach number increases beyond this, the large-scale structures in the mixing layer become more three dimensional and less organized,[8,9] and the convective velocity can deviate considerably from Eq. (1).[10] For a Mach 1.3 jet, the theoretical convective velocity and Mach number are 200 m/s and 0.6, as computed with Eqs. (1) and (2).

Murakami and Papamoschou[11] found an empirical relation for the convective velocity at higher speeds. For a supersonic jet, without

Received 30 August 2000; revision received 15 February 2001; accepted for publication 22 February 2001.

*Graduate Student, Department of Mechanical Engineering. Member AIAA.
†Professor, Department of Mechanical Engineering. Associate Fellow AIAA.

a coflow, the average convective velocity can be computed with the following empirically based equations:

$$u_c = -M_{cj} a_j + u_j \tag{3}$$

$$M_{cj} = M_c + \frac{-dM_c}{\sqrt{1 + (a_j/a_0)^2}} \tag{4}$$

$$dM_c = 1.25\,\ln(M_c) + 1.11 \tag{5}$$

where dM_c is the convective Mach number deviation. When these relations are used, the average convective velocity of a Mach 1.3 jet without coflow is approximately 300 m/s. There is a considerable discrepancy between the theoretical value from Eq. (1) and the one from Eq. (3). The results of Murakami and Papamoschou[11] have been further supported by the detailed experimental results of Thurow et al.[12] The results of Thurow et al. were obtained in the same jet facility as the current work using real-time flow visualizations. Thus, the convective velocity will be assumed as 300 m/s for this study.

For subsonic or ideally expanded supersonic jets, the dominant noise source is expected to originate from the turbulence structures within the mixing layer. If the convective velocity of the large-scale structures is subsonic, then this component of jet noise is commonly referred to as turbulent mixing noise. However, if the convective velocity is supersonic relative to the ambient, then the large-scale structures will emit Mach wave radiation. Because the convective Mach number for the jet in this study is subsonic, Mach wave radiation should be insignificant, and as such the focus will be on turbulent mixing noise.

Turbulent mixing noise is known to be highly directional within the acoustic far field, with peak noise emission occurring at angles close to the jet axis. This preferred angle has been measured to vary from 25 to 45 deg with respect to the jet axis.[13] The peak frequency of the noise spectrum at this angle has been found to vary from a Strouhal number based on jet diameter, St_D, of 0.16 to 0.33 for high subsonic and low supersonic jets.[14–16] The majority of the turbulent mixing noise production emanates from a region around the end of the potential core. This determination has been made by measuring the noise intensity globally over the acoustic near field.[13,14,17] A measurement of the acoustic phase fronts also supports this finding.[14] When the correlation between the velocity fluctuations inside the jet and the far-field acoustic pressure is used, the noise sources of a Mach number 0.98 jet were determined to originate from the region of the jet between 5D and 10D (Ref. 18). Through the utilization of various microphone arrays, several researchers have found that for high subsonic jets the high-frequency noise is generated near the exit of the jet, whereas lower frequency noise originates farther from the jet exit.[16,19,20]

Some work has been conducted to relate structures in the flow to the jet acoustic field. Sarohia and Massier[21] performed experiments with high-speed schlieren motion pictures that were synchronized with near-field pressure measurements. They studied excited subsonic jets with Mach numbers ranging from 0.1 to 0.9 with a Reynolds number of approximately 10^6. They found that large instantaneous pressure pulses were formed whenever two large-scale structures merged; however, the passage of a large structure did not significantly change the near-field pressure signal. Morrison and McLaughlin[14] found the dominant noise production mechanism within three low-Reynolds-number jets (Mach numbers 1.4–2.5) to be the rapid growth, saturation, and decay of instability waves near the end of the potential core. They conjectured that the majority of the noise is due to the rapid decay (disintegration) of the instability waves, and this disintegration involves a "relatively violent fluid dynamic action."

There has also been a substantial amount of work conducted in low-speed jets to relate vortex pairing to turbulent jet noise. In one such example, Kibens[22] excited the shear layer of a low-Reynolds-number ($Re = 5 \times 10^4$), low-speed jet at the shear layer instability frequency. The forcing caused large-scale structures to form at the frequency of the forcing. The regular vortex pairing that resulted caused the far-field noise spectrum to change from broadband to being dominated by discrete frequencies (at the forcing frequency and its subharmonics). These subharmonics corresponded to the frequencies at which the large structures were pairing. However, Hussain[3] argues that vortex pairing is probably not the principal mechanism for jet-noise generation in practical jets with large Reynolds number. This argument relies on the fact that initially turbulent jets do not generally experience vortex pairing. Instead, Hussain argues that the dominant noise generation mechanism is due to the breakdown of the torroidal structures that encircle the core of the jet near the end of the potential core and the subsequent interactions between the substructures.[3,23] One conclusion that can be made from all of the reported work is that the mechanism of turbulent mixing noise generation involves nonlinear interactions between large-scale structures.

The work of this paper is an initial part of an ongoing attempt to relate large-scale turbulence structures to turbulent mixing noise. The jet in this study is axisymmetric with a Mach number of 1.3 and a Reynolds number of 10^6. This study was carried out in the following way. First, the structure of the jet in the area surrounding the end of the potential core was examined because this seems to be the dominant area of noise production. Then, the far-field acoustics of the jet were analyzed in time and frequency, with the emphasis on the preferred noise emission direction for the turbulent mixing noise. Finally, the two measurements were brought together in an attempt to relate the flow structure to the far-field acoustic radiation.

Experimental Arrangement

All of the experiments were conducted in the recently constructed optically accessed anechoic chamber of the Gas Dynamics and Turbulence Laboratory (GDTL) of The Ohio State University. Instantaneous, streamwise flow visualizations and far-field sound pressure measurements were taken separately and simultaneously. Explanations of the experimental setup and data reduction techniques, beyond those presented here, can be found in Hileman.[24]

Jet Facility

The air for the jet is supplied by two four-stage compressors; it is filtered, dried, and stored in two cylindrical tanks with a total capacity of 42.5 m^3 at 16.5 MPa (1600 ft^3 at 2500 psi) pressure. The air is delivered to a stagnation chamber that is 0.24 m (9.5 in.) in diameter and 0.91 m (36 in.) long for flow conditioning. The air passes through a perforated plate [0.6-cm ($\frac{1}{4}$-in.) holes, 37% porosity] and two 55.4% open mesh screens. After the second mesh screen, a converging cone funnels the air into a 0.41-m- (16-in.-) long, 6.0-cm- (2.35-in.-) diam pipe that connects to the axisymmetric nozzle. The exit diameter of the nozzle was 2.54 cm (1 in.), and it had a lip thickness of 0.25 cm (0.1 in.). The inner nozzle contour was determined by the method of characteristics for uniform flow at the exit. The actual Mach number of the nozzle was measured as 1.28 using a pitot probe.

Anechoic Chamber

The optically accessed anechoic chamber has been designed and constructed to investigate acoustic radiation from high-speed jets. This modular anechoic chamber allows for the simultaneous measurement of acoustic radiation and flow parameters using a variety of optical diagnostic techniques. A schematic of the facility, as seen from above, is shown in Fig. 1. The inner dimensions of the chamber from wedge tip to wedge tip are 3.1 m (122 in.) in width and length, and 2.7 m (106 in.) in height. Because of the flexibility of the structural beams used to create the skeleton of the chamber, sections can be removed from all four walls. An open area has been built around the perimeter of the front wall of the chamber to allow for adequate airflow into the chamber for entrainment by the jet. The chamber was tested for compliance to American National Standards Institute Standard S12.35, and the results from the tests were within the required tolerance over most of the distances along the microphone paths.[25,26] B & K Model 4135, $\frac{1}{4}$-in. microphones were used to measure sound pressure levels in the chamber, and the data were electronically low-pass-frequency filtered at 125 kHz. For spectral analysis, the data were also filtered via software. Further details of the anechoic chamber may be found in Refs. 25 and 26.

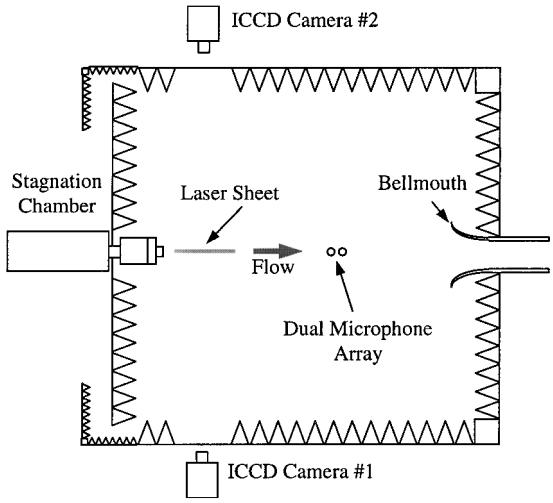

Fig. 1 Schematic of the optically accessed anechoic chamber.

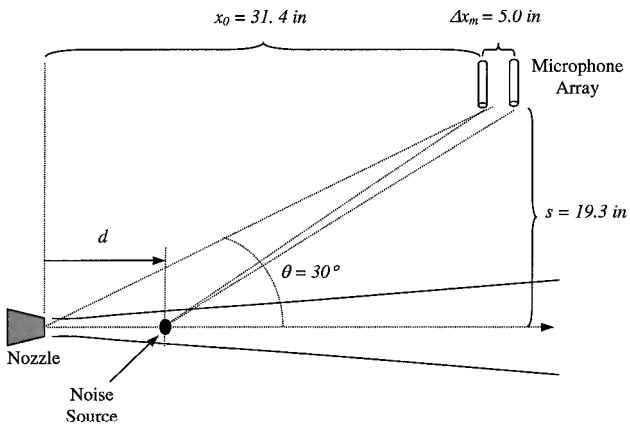

Fig. 2 Schematic of the dual microphone geometry used to determine noise source location.

Dual Microphone Array

A simple dual microphone array was used to determine the approximate spatial and temporal location of intense sound sources within the jet. The location of the microphone pair was chosen to coincide with the angle of preferential noise emission for the large-scale turbulent structures within the flow. The microphone pair was attached to the ceiling of the anechoic chamber at an approximate angle of 30 deg from the jet axis. This is shown in the schematic of Fig. 2. The relevant dimensions are also given in Fig. 2. When the amount of time is measured between a given sound wave reaching the first and then the second microphone the location from which the sound wave originated can be determined. This location is then used to calculate the distance d from the sound source to the exit of the jet nozzle. The noise source is assumed to be located on the jet centerline. The relation between the geometry of the dual microphone array, the time separation between a sound wave reaching the two microphones τ, and the location of the noise source d is given implicitly by

$$\tau a_0 = \sqrt{s^2 + (x_0 + \Delta x_m - d)^2} - \sqrt{s^2 + (x_0 - d)^2} \qquad (6)$$

or equivalently

$$d = x_0 + \frac{\Delta x_m}{2} - \frac{\tau a_0 s}{\sqrt{\Delta x_m^2 - \tau^2 a_0^2}} \qquad (7)$$

where a_0 is the speed of sound within the ambient air and the other terms are defined in Fig. 2.

The time separation was computed using cross correlation of the two microphone signals. A 0.38-ms segment from the front microphone that contained the sound peak of interest at its center was chosen, and then an equally long time segment from the second microphone signal was scanned to determine the maximum cross correlation. The time delay associated with the maximum cross correlation was used as the time separation. With a sampling rate of 400 kHz, a segment length of 0.38 ms corresponds to 150 data points. This length was chosen because it would contain only a single large-amplitude pressure pulse; therefore, only the origin of that sound waveform would be determined. Because this technique is used to find the instantaneous location of a noise source using a single pressure peak, there should not be any Doppler shift effects on the noise source location because the Doppler shift affects the wavelength of a wave train. The use of cross correlation is a more accurate means of determining the time separation than the technique used in Refs. 24 and 27. That is because cross correlation utilizes the entire pressure peak, whereas the difference between the local maxima or minima of the two microphone signals was used in Refs. 24 and 27 to determine the time separation.

There are several places where error could influence the noise source location technique. Three main sources are discussed here. The first error source is in the measurement of the time separation τ. The sound data were acquired at the rate of $f_s = 400$ kHz. Therefore, there is a period of 2.5 μs between successive data points, and as such there is an error of ± 2.5 μs in the measurement of the time separation. The second possible error source arises from the vertical location of the noise source because it could be either above or below the jet centerline. The maximum distance a noise source could vary from the jet centerline is approximately one nozzle radius ($\pm D/2$). For example, if the source were $D/2$ above the jet centerline at a streamwise (downstream of the nozzle exit) location of $8.9D$, then the noise source would appear to be at a streamwise location of $8.2D$ on the jet centerline. The effect of the vertical source location was demonstrated experimentally by Hileman et al.[28] The sideline microphone distance s was, therefore, modified by $\pm D/2$ for a given time separation in Eq. (7) to determine the range of streamwise locations that would result. When the effects of the first two possible errors are combined, the location of noise emission for a time separation of 0.2925 ms would be $8.9D$ with an error of $\pm 1.2D$. The third error source is due to the uncertainty in the measured geometry of the experimental setup and the ambient air temperature. The air temperature within the anechoic chamber determines the propagation velocity of the sound waves and was measured at 294 K with an assumed uncertainty of ± 2 K. The microphone array geometry measurements s, Δx_m, and x_0 were assumed to be in error by ± 0.15, ± 0.15, and ± 0.25 cm, respectively. Adding the effects of the ambient temperature and array geometry to the other error sources yields a location of $8.9D$ with an error of $\pm 2.5D$ for a time separation of 0.2925 ms.

This simple analysis assumed negligible refraction of the sound waves within the jet mixing layer and negligible phase distortion of the target noise source due to the effects of other noise sources. The authors realize these shortcomings in the analysis. Potential effects of these assumptions will be addressed as needed in this paper, while work is being carried out to correct these error sources. Note that no assumption has been made on the nature of the noise source and whether it is compact or not. It is assumed that a noise source in the jet generates a pressure pulse that gets radiated to the far field. The time separation between the peak of this pulse reaching the front and the back microphone together with the geometrical information in Fig. 2 are used in Eq. (6) or (7) to determine the streamwise location of the noise producing event. However, this technique introduces an uncertainty, due to the neglect of the lateral dimension, the extent of which was discussed earlier.

To relate an intense noise emission event to large-scale turbulence structures that were captured within flow visualization images, one has to be able to relate the time of noise emission to when the flow structure was captured by the visualization. Rarely will the laser illuminate the flow while a sound wave is being produced. The laser will probably illuminate the evolving flow events in the jet mixing layer, either before or after the noise generation occurred. Therefore,

one needs to measure the time lag between the flow visualization and the emission of the sound wave by the noise source. This time lag t_L is given by

$$t_L = t_m - \sqrt{s^2 + (x_0 - d)^2}\,/a_0 \tag{8}$$

where t_m is the amount of time between the laser illuminating the flow and the peak of the sound wave reaching the front microphone. The value of t_m is known because the sound acquisition is triggered by the laser illumination. With the computed time lag using Eq. (8), the computed noise emission location using Eq. (7), and the assumed convective velocity of the large-scale structures, the region of the mixing layer during laser illumination that was responsible for noise generation can be determined. It is given by

$$d_{\mathrm{LF}} = d - u_c t_L \tag{9}$$

where d_{LF} is the expected location of the noise producing region during the first flow image. Thus, this technique will be used to determine the streamwise location and time (with respect to the acquired flow image) of a noise producing event.

Flow Visualization

The flow visualizations utilized the commonly used planar Mie scattering technique. The mixing layer, which is formed between the ambient air and the high-speed jet flow, was marked by condensed moisture from the ambient air that was entrained into the jet mixing layer. The laser used in the experiments was a Continuum Powerlite 8010 Nd:YAG laser operating at a wavelength of 532 nm in either single- or double-pulse mode. The laser was located outside of the chamber in all of the experiments, and the beam from the laser was redirected into the chamber through a 2.5-cm hole in one of the large structural beams of the anechoic chamber. A framework connected to the ceiling of the anechoic chamber held the optical components that were used to create the laser sheet. The framework was covered with acoustic foam to minimize acoustic reflection. The laser sheet passed through or normal to the jet centerline thus illuminating the flow either in the streamwise or the cross stream direction. Two Princeton Instruments integrated charge-coupled device cameras were placed outside of the chamber, perpendicular to the laser sheet, to capture images of the flow. The cameras had visual access to the jet flow via holes cut into two foam sections that were put in place of the removable anechoic wedges. A schematic of the experimental arrangement showing the laser sheet and camera positions relative to the jet was given in Fig. 1.

Results and Discussion

Flow Images

Initially, several sets of single-pulse images were taken that covered a range of the jet from 4.5D to 9.5D. This spans the region upstream of the end of potential core where the two sides of the mixing layer are separated by the potential core to downstream of where the two sides have merged. The average and rms of 25 such images are shown, respectively, in Figs. 3 and 4. In the images, both the ambient and the core region of the jet are dark because they do not contain scattering particles. The rms image shows the level of intermittency in the mixing layer at a given location. In other words, the intensity of the rms image is directly related to the large-scale fluctuations in the mixing layer; therefore, the areas with maximum intensity are also the areas in which the most activity occurred between mixed and either ambient or core flow of the jet. The areas between these two extremes have a lower rms intensity, thus showing less intermittency. The average image shows the two sides of the mixing layer merging between 6D and 9D. This is also the area of maximum intensity in the rms image.

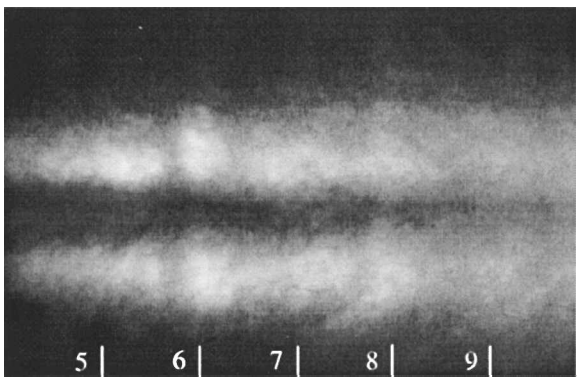

Fig. 3 Average of 25 flow images; tic marks indicate the streamwise distance from the nozzle exit, in jet exit diameters.

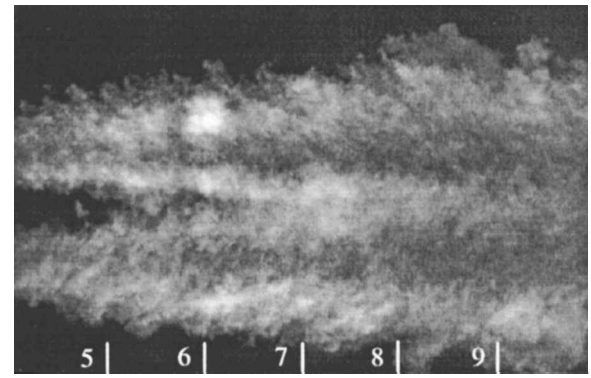

Fig. 4 RMS of 25 flow images.

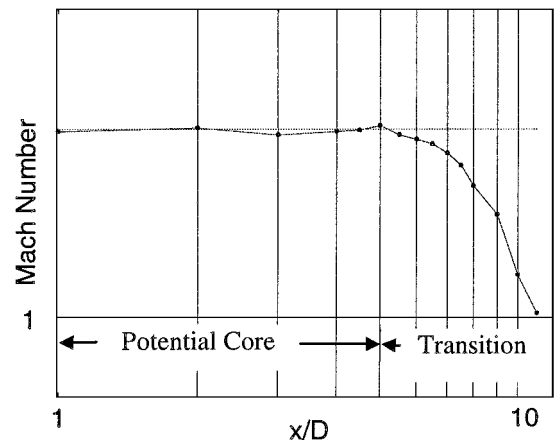

Fig. 5 Centerline Mach number vs streamwise distance.

As stated in the Introduction, a large portion of the noise emitted by a jet has been found to originate around the end of the potential core. The instantaneous, average, and rms flow visualizations can give an idea of where the end of the potential core is located; however, these results are subjective because they mark a major portion but not the entire mixing region. This is due to the nature of the condensation process. For these reasons, the end of the potential core was measured quantitatively with a pitot tube placed on a traversing mechanism. The flow was interrogated from the jet exit to a distance of 11 jet diameters downstream. The pitot pressure was measured with a mercury manometer, and the pressure at the jet exit was assumed to be equal to the ambient pressure because the jet was operating in the ideally expanded regime. As seen in Fig. 5, the centerline Mach number starts to decrease between 5 and 6 jet diameters. This marks the end of the potential core. At this point, on average, the mixed ambient/freestream fluid has reached the center of the jet. Lepicovsky et al.[29] measured the centerline velocity of a Mach number 1.38, Reynolds number 1.6×10^6 jet using a laser velocimeter and found it started to deviate from a constant value between 5D and 7D. Other researchers[17,30,31] measured a similar value for the end of the potential core within a Mach 1.5 jet.

Double-pulse instantaneous flow visualizations were taken to gain a better understanding of the dynamics of large-scale structures in the jet. Two sets of data are presented here, and many more sets can be found in Ref. 24. Figures 6 and 7 show the mixing layer of the jet from 4D to 9D with a time separation of 100 μs between

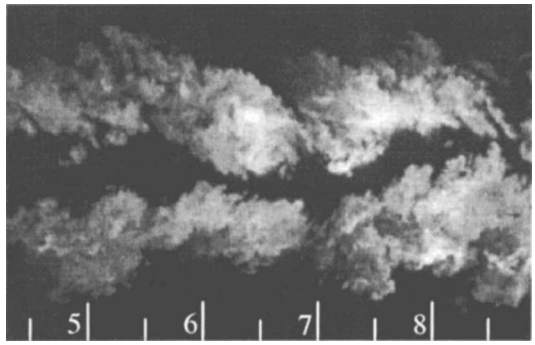

Fig. 6 First pulse flow image ($t = 0$ μs) showing a pair of structures before pairing.

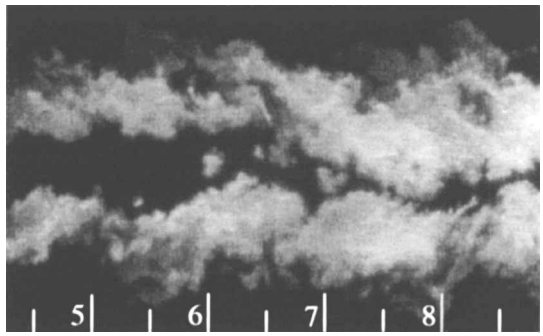

Fig. 7 Second pulse flow image ($t = 100$ μs) showing the structures after pairing.

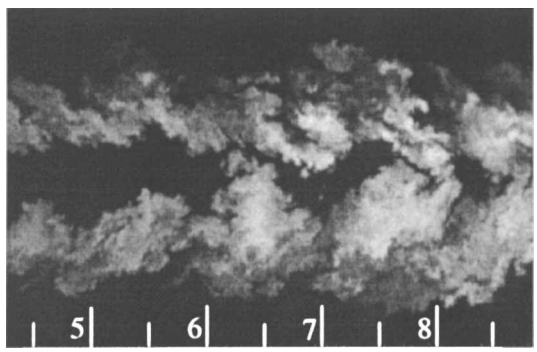

Fig. 8 First pulse flow image ($t = 0$ μs) showing the merging of structures between 6*D* and 7.5*D*.

the images. With an assumed convective velocity of 300 m/s, the structures should convect 1.2*D* between the two images. In the first image, there are four structures around 7*D* (a set of two above the jet centerline, another set below). This could indicate the existence of a pair of axisymmetric structures with a braid located between them around 7*D*. In the second image, the two sets of structures have nearly merged into a single seemingly axisymmetric structure that extends from 7*D* to about 8.5*D*. It appears that the two structures have merged because the upstream structure, being closer to the center of the jet, was moving faster and overtook the slower, downstream structure. It also appears that the nearly merged structure is collapsing on itself, thus pinching off the unmixed core of the jet. One would expect this process to be a potential noise source within the jet.

In Figs. 8 and 9, portions of the top and bottom sides of the mixing layer have merged over a time span of 100 μs. In Fig. 8, there are two separate structures on the bottom-half of the mixing layer centered, respectively, at 6.5*D* and 7.5*D*. There is also a structure in the top-half of the mixing layer centered at 7*D*. In Fig. 9, which was taken 100 μs later, the space between the three structures has dramatically decreased and there is a thin line of unmixed fluid that extends from 8*D* to 8.5*D*. The three structures have nearly merged into a solid mass of fluid. Obviously, this is also an area of intense interaction

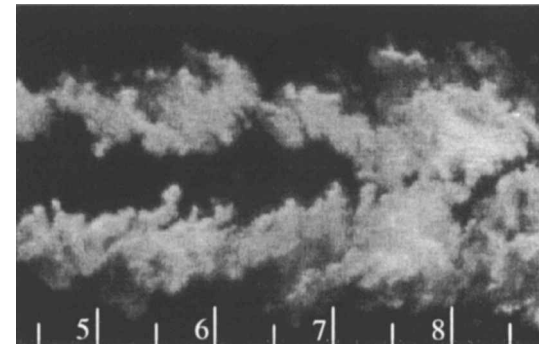

Fig. 9 Second pulse flow image ($t = 100$ μs) showing the merged structures between 7.5*D* and 9*D*.

between the two sides of the mixing layer and a potential acoustic source. Note that this is an asymmetric interaction, unlike that of the preceding example, where the structure interaction was symmetric with the jet axis.

Instantaneous images were also taken in the cross stream direction. Figure 10 shows four typical images taken at streamwise locations of 3*D*, 5*D*, 7*D*, and 9*D*. The three-dimensional nature of the jet is quite obvious, with ejection and entrainment of fluid observed at all four locations. As expected, the unmixed core of the jet decreases in size while the mixing layer increases in size with increasing streamwise distance. Although not shown, downstream of 5*D*, the unmixed core of the jet drifts significantly with respect to the jet centerline from one image to another.[24] It was observed that the unmixed core of the jet disappears in a few of the instantaneous images taken at 8*D* (not shown here), but the unmixed core was nonexistent in almost every image taken at 11*D* (Ref. 24). The average images (not shown here) show a typical ring-type mixing layer. More cross stream images at these and other streamwise locations can be found in Ref. 24.

In all of the single- and double-pulse flow images, there were structures of various sizes on both sides of the mixing layer that were either evenly spaced or staggered with the structures on the opposite mixing layer. However, there were no visually apparent interactions between the two sides of the mixing layer upstream of approximately 6*D*. Farther downstream, both symmetric and asymmetric interactions occurred between the two sides of the mixing layer. These interactions marked the end of the unmixed central core of the jet. In the asymmetric interactions, the braid between two large structures on one side of the mixing layer matched up against the core of a structure on the other side of the mixing layer. This caused the unmixed core of the jet to have a wavy appearance, perhaps an indication of a helical structure. In the symmetric cases, a structure within one side of the mixing layer interacted with a structure at the same streamwise location within the other side of the mixing layer. This often led to unmixed fluid at the core of the jet becoming surrounded by mixed fluid on all sides or pinched off. In most cases, the initial interaction between the two sides of the mixing layer occurred between 6*D* and 7*D*, but the end of the unmixed fluid core ranged from 7.5*D* to 9.5*D*. Thurow et al.[12] obtained real-time flow visualization movies of this jet at the same operating conditions in both the streamwise and cross stream directions. They observed all of the aforementioned phenomena, but they were able to better describe the processes because they had up to 17 real-time images showing the development of the mixing layer instead of one or two as in the present work.

Acoustic Results

The acoustic far field was measured at various angles with respect to the jet axis to determine the peak noise emission direction for the Mach 1.3 nozzle. This was done by placing a series of microphones at 10-deg increments along a line that was parallel to and 30*D* from the jet axis. The spectra for selected angles between 20 and 90 deg are shown in Fig. 11. The orientation with which the angles were measured is also shown in Fig. 11. The spectra were created from 100 blocks of 32,768 samples of noise data that were taken at a data acquisition rate of 140 kHz. The amplitudes of all of the spectra were

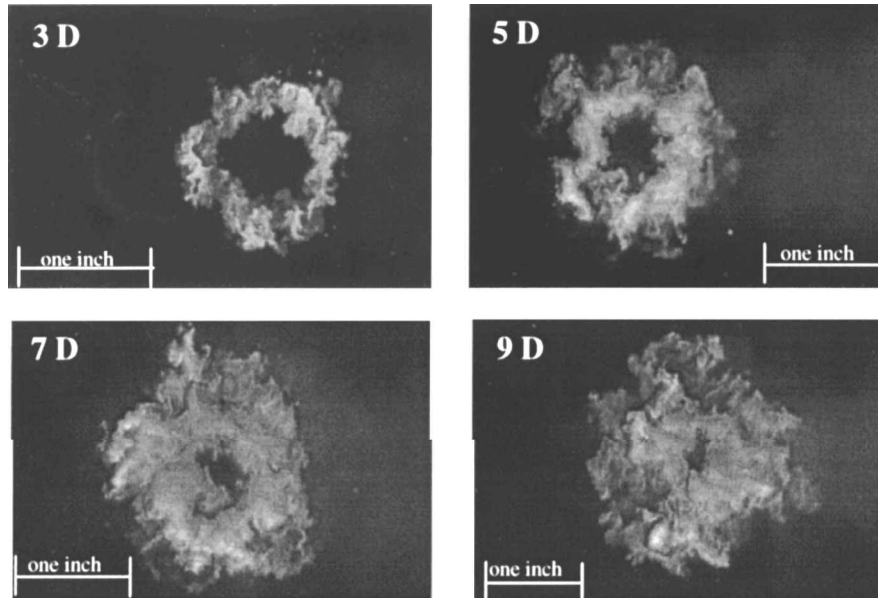

Fig. 10 Typical, instantaneous, cross stream images taken at locations of 3*D*, 5*D*, 7*D*, and 9*D*; size of the jet nozzle exit is given by the scale.

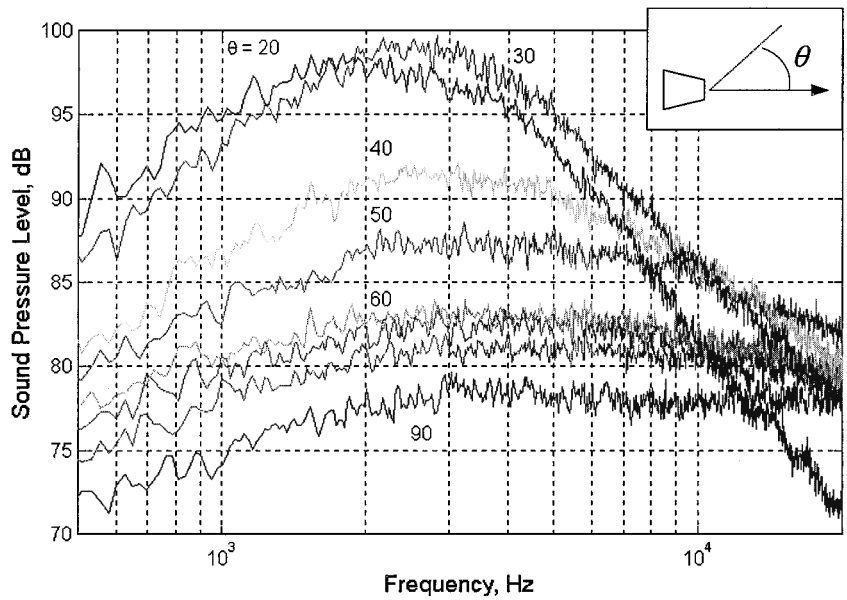

Fig. 11 Variation in the far-field acoustic spectra with changing observation angle θ.

adjusted to 60*D* by decreasing the sound intensity by 6 dB for every doubling of distance. The frequency peak has maximum amplitude at an observation angle of 30 deg. This was also the angle where the overall sound pressure level peaked.[24] The peak frequency at 30 deg was measured at about 3 kHz. This gives a Strouhal number Sr_D of about 0.2 for a jet diameter of 2.54 cm and a centerline exit velocity of 375 m/s. The angle of the peak noise emission matches that for a high-Reynolds-number Mach 1.5 jet[17] and a low-Reynolds-number Mach 1.4 jet.[14] Once the peak noise emission direction was determined, all of the other acoustic measurements were made at that angle.

Traditionally, sound pressure data are examined after they have been Fourier transformed and averaged over extended periods of time to obtain spectral information. In the conversion of the data to the frequency domain, the sound data lose their temporal character, which is needed to relate the instantaneous flow structure to large-amplitude sound events. In the current work, the sound pressure data are treated in an unconventional manner because they are investigated in the time domain. Short segments of time traces were analyzed to determine the temporal contents of the acoustic data and how various features of the acoustic signature relate to the development of turbulence structures and their interaction in the flow. In the current work, we have used time traces directly; in future work, more advanced time–frequency analysis will be utilized.

A sample time history of the sound pressure for both of the microphones within the array is presented in Fig. 12. All of the time traces that will be presented were acquired at a rate of 400 kHz. The time traces show how the sound pressure fluctuates over short periods of time, and with simultaneous flow visualization, some of the distinct fluctuations can then be related to the turbulence structures in the jet. An example of such a set of fluctuations is between 1.5 and 2.3 ms of Fig. 12, where the sound pressure alternates from negative to positive to negative again with a period of approximately 0.3 ms. The negative sound pressure peaks within this oscillatory series have been marked C–E in Fig. 12. The peaks marked A and B were not included in this group of oscillatory peaks because they seem to be out of phase with the other peaks. The positive peak B occurs about 0.28 ms before the negative peak C, and peak A is only about 0.09 ms before event B. Thus, peaks A and B were probably not produced by the same phenomenon that created events

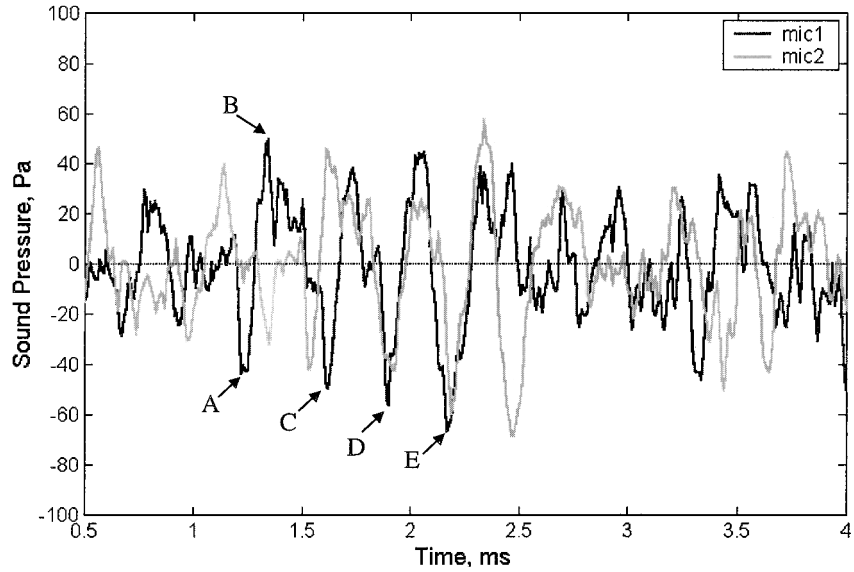

Fig. 12 Time trace of the microphone array data showing a series of oscillatory sound pressure peaks.

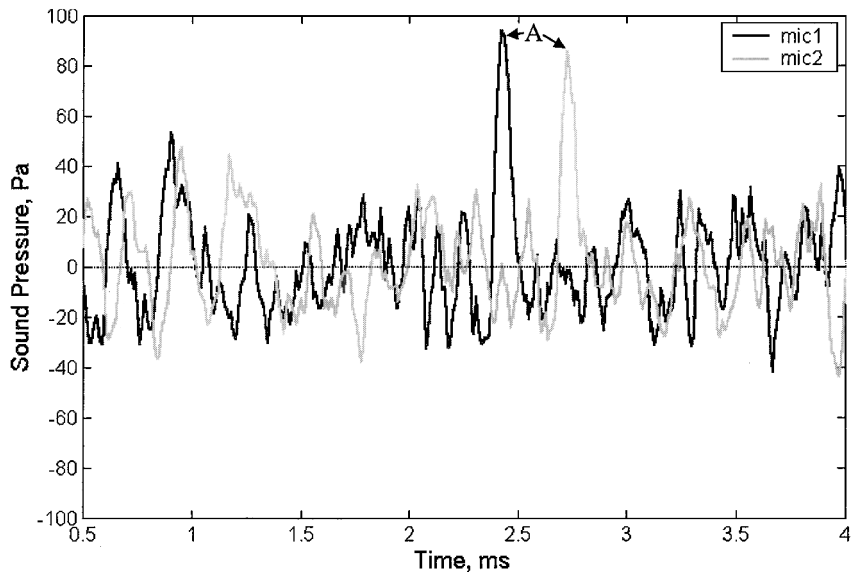

Fig. 13 Time trace of the microphone array data showing a single peak and relative quiet periods.

C–E. By further examining the time range from 1.5 to 2.3 ms in Fig. 12, one can see the magnitude of the peaks increases with time. In many other similar sets of peaks, there is also a period of time after the largest peak where the magnitude of the peaks decreases with time. Groups of oscillating large-amplitude peaks, similar to those between 1.5 and 2.3 ms in Fig. 12, were observed in many other acoustic time signatures.

In addition to the expected groups of oscillating, large-amplitude, seemingly related, peaks, there were also individual large-amplitude peaks. Figure 13 shows an example of such a large-amplitude, sound pressure event. This event, marked A, is a positive pressure fluctuation with a magnitude of 95 Pa. This noise event is very similar to the crackle phenomenon observed by Ffowcs Williams et al.[32] in the Olympus engines used in the Concorde. They observed that the Olympus engine created a series of sharp compressions (positive pressure peaks), crackles, that were followed by gradual expansions. A typical series of compressions as measured by Ffowcs Williams et al. consisted of about 10 peaks, and this could persist up to 0.1 s. The strength of the compressions was about 500 Pa at a distance of 50 m. They used the skewness of the sound data as a measure of crackle. If the skewness was less than 0.3, the jet was not considered to be crackling, whereas a jet with skewness in excess of 0.4 was crackling distinctly. They attributed the crackling phenomenon to nonlinearities at the source and not to nonlinear wave propagation. To confirm whether or not the current jet was crackling, a statistical analysis was performed on the sound pressure data from both of the microphones within the array. Figure 14 shows a histogram of the sound pressure data from the two microphones within the array. The distribution appears to be Gaussian, and the computed skewness is under 0.1, which is well below the criteria set by Ffowcs Williams et al.[32] Thus, these large-amplitude events are not considered to be crackle by the given definition. This is consistent with the work of Ffowcs Williams et al. because they found a similar Mach number jet did not crackle.

In Fig. 13, the time range from 1.0 to 2.0 ms for the front microphone has no peaks in excess of 30 Pa, which corresponds to 1.5 times the standard deviation σ of the microphone sound data. This is a large period of time without any significant sound events. To give a physical meaning to a 1-ms time period, a large-scale structure traveling at 300 m/s (the convective velocity obtained experimentally for the current jet[12]) would convect nearly $12D$ over this time period. There are similar periods of relative quiet (defined as having no sound pressure peaks in excess of 1.5σ) in the front microphone time traces of Fig. 12 between 2.5 and 3.3 ms and of Fig. 13

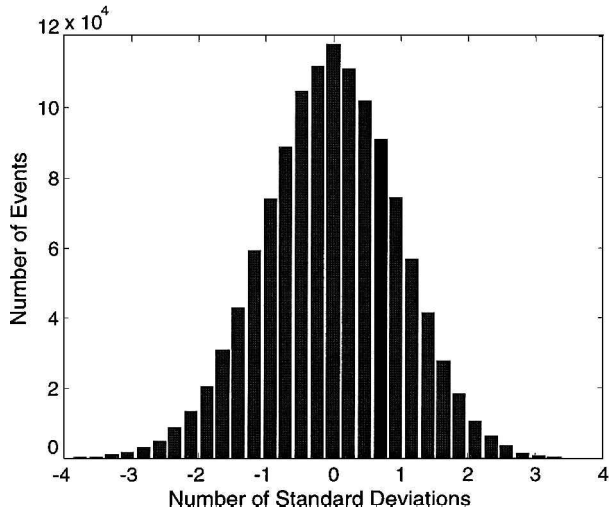

Fig. 14 Histogram of the magnitude of the microphone array data.

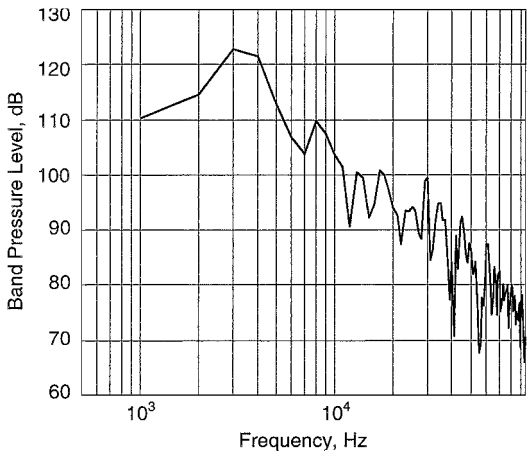

Fig. 15 FFT of the time range of 1.5–2.5 ms of Fig. 11 that contains a series of periodic peaks.

between 2.5 and 3.1 ms, in addition to many other data sets not shown here.

These results are typical of all of the far-field measurements taken at the peak emission microphone location of 30 deg. There were time signatures that have individual peaks or periodic peaks, and there were significant periods without any large peaks. In some instances, all three occur over a range of a few milliseconds. These results indicate that there exist various mechanisms within the jet that create individual or repeating large-amplitude noise events, and at other times there is no mechanism present that would create intense noise at the 30-deg location.

These individual noise features were also analyzed in the frequency domain by converting small segments of the time signatures into spectra via fast Fourier transformation (FFT). Each segment consisted of 400 data points covering a 1-ms time period. The spectra can then be compared to the spectrum taken at 30 deg obtained by averaging 100 blocks of 234-ms time segments, which was shown in Fig. 11. The frequency spectra from the three time segments that were observed in Figs. 12 and 13 are shown in Figs. 15–17. Figure 15 shows the spectrum for the time range between 1.5 and 2.5 ms that contains a series of oscillating sound pressure peaks in Fig. 12. There is a relatively well-defined peak in the spectrum around 3 kHz that matches the overall peak of the sound data at 30 deg in Fig. 11. Similar sets of oscillatory peaks were found to have a frequency between 2 and 5 kHz. Figure 16 shows the FFT of 1 ms of the time trace of Fig. 13 that has the large peak of 2.43 ms at its center. Unlike the spectrum in Fig. 15, there is no well-defined peak in this case. This should not be surprising because there were no sound pressure oscillations before or after the peak. Most of the spectra that came from time signatures containing a single large-amplitude

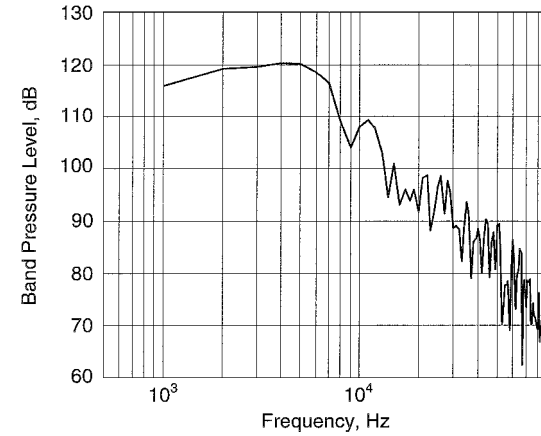

Fig. 16 FFT of the time range of 1.5–2.5 ms of Fig. 12 that contains a single peak in time trace.

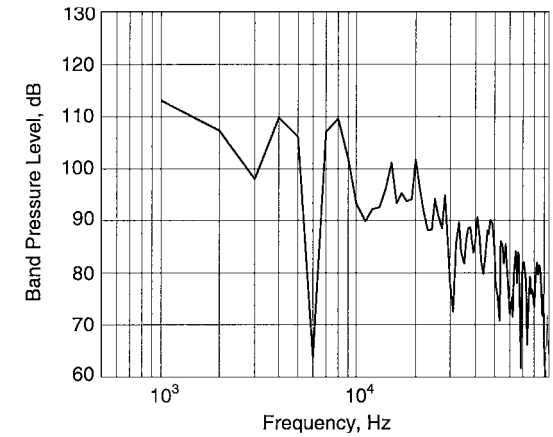

Fig. 17 FFT of the time range of 1.0–2.0 ms of Fig. 12 that contains no large peaks.

sound pressure peak have a moderate amplitude plateau, similar to the one of Fig. 16. The spectrum of Fig. 17 is from the relatively quiet portion of Fig. 13 between 1.0 and 2.0 ms. As expected, this spectrum has relatively low amplitude at all frequencies, which is consistent with spectra from other relatively quiet periods.

The fractions of time the jet is producing the various events just discussed need to be quantified to assess whether these events contribute substantially to noise radiation and whether there is hope of reducing the overall jet noise by altering the mechanisms that create these noise events. When some criteria are set for each of the noise events, it is possible to determine the percent of time the microphones were recording each of the noise event types. First, the sound pressure data were analyzed for all large-amplitude events that were in excess of 2σ (42 Pa). The length of time that the microphones were recording these large-amplitude peaks was defined to be the time period between when the sound pressure crossed zero before the peak and when it crossed zero again after the peak. With this definition, the microphones were recording large-amplitude events, in excess of 2σ, 23% of the time.

Second, the percent of time the microphones were recording periodic noise events was determined. This was accomplished with another set of criteria. This time, the data were analyzed to determine how much time was spent creating a set of three or more peaks and valleys constituting a complete cycle. All of the peaks were required to have amplitude above a set value and a frequency between 2 and 5 kHz. The time period between a peak and a valley within the three-peak/valley set also had to be within 25% of each other. The microphones were recording sets of periodic peaks, all in excess of 2σ, only 2% of the time. Apparently, there are many large peaks in excess of 2σ, but only on rare occasions are there three or more peaks and valleys, all having amplitudes above 2σ, which form a cycle. If the amplitude threshold was lowered to 1.5σ, the jet

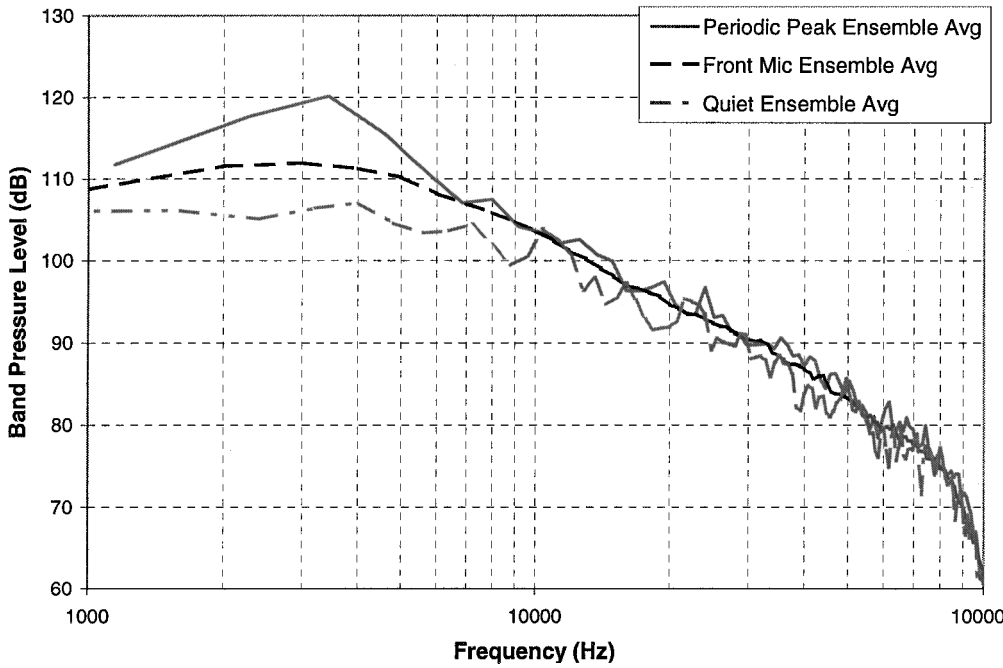

Fig. 18 Comparison of the spectra from periodic peaks, average, and relatively quiet sets of data.

produced series of periodic peaks 8% of the time. This is a considerably larger amount of time. Note that in many time signatures, there were several peaks that had a period meeting the stated criteria, but one of the peaks was below the 1.5σ threshold value. These types of periodic events were not included in the periodic peak percentages.

Finally, the fraction of time the microphones were recording a period of relative quiet was determined by defining a minimum length of time and a maximum allowable sound pressure level. The relative quiet periods were defined not to have any peaks in excess of 1.5σ, and the minimum time length was set to correspond to a large structure either convecting $5.9D$ (0.5 ms) or $11.8D$ (1.0 ms). This convection time assumes that the large-scale structures travel with a convection velocity of 300 m/s. When a time period is used that corresponds to crossing zero heading into the relative quiet time segment and leaving the relative quiet segment, the percent of time in a relative quiet mode was either 22% (for $5.9D$) or 6% (for $11.8D$). This means that about 6% of the time a large-scale structure could have traveled twice the length of the potential core without producing any significant sound pressure pulses in the direction of the microphone array. Nearly one-fifth of the time, a structure could have traveled the length of the potential core without producing any significant sound pressure events in the 30-deg direction.

The ensemble spectra from two of the different types of noise events are plotted with the average spectrum in Fig. 18. Figure 18 shows the ensemble average of 14 spectra taken from relatively quiet periods, the ensemble average of 24 spectra taken from periodic peak noise events, and the overall ensemble average spectrum of 300 sets of sound data taken at the same location. Performing an FFT on the first 400 data points of each data set of 32,768 data points and then averaging these short spectra created the overall ensemble average spectrum. The single peak data were not plotted because these spectra were found to vary considerably from one data set to the next. Beyond approximately 10 kHz, there is no difference between the three spectra. However, at lower frequencies, the relatively quiet spectrum has a lower amplitude than the average spectrum, and the periodic peak spectrum has a large peak centered at approximately 3 kHz. At 4 kHz, the overall ensemble average spectrum has a value of 111 dB, whereas the relatively quiet ensemble average spectrum has a value of 107 dB, and the periodic peak ensemble average value was about 117 dB. If it were possible to eliminate the periodic peak noise generation mechanism, then the jet noise radiation could potentially be reduced considerably.

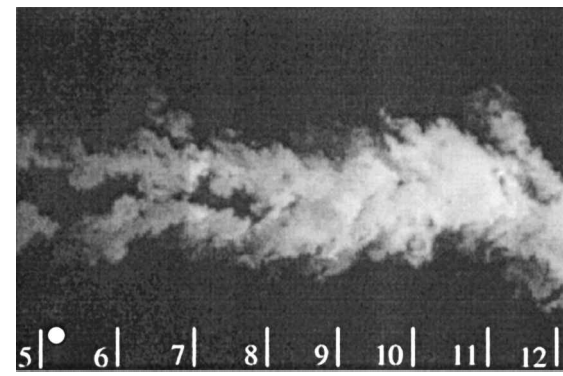

Fig. 19 Simultaneous first flow image for the time trace of Fig. 13; time = 0 μs.

Simultaneous Flow/Acoustic Results

The simultaneous measurements combined all of the techniques that have been described thus far, along with the noise source location technique described in the experimental setup section. These measurements incorporated double-pulse flow visualization with far-field acoustic measurements from two closely spaced microphones. The sound pressure time traces from the front and the rear microphones of the dual microphone array were used to determine the location of the noise sources. All three of the data sets presented here have noise events that would classify as single large-amplitude events.

The time trace shown in Fig. 13 was from a simultaneous data set. Based on the time difference between when event A reached the front and rear microphones ($\tau = 0.3025$ ms), event A was determined to originate near $6.3D$ and was created approximately 92 μs after the first flow image was taken ($t_m = 2.4275$ ms). Figure 19 is a flow visualization image that was taken at time zero with respect to the time axis of Fig. 13. Figure 20 is a flow visualization image that was taken 60 μs later. In the first flow image, the region of the jet that eventually generated the noise event A was located at about $5.3D$, and this region is at approximately $6.0D$ in the second image. These areas are marked with a dot at the appropriate streamwise location. The $5.3D$ location within the first image contains a structure within the top-half of the mixing layer. In the second image, the structure has grown considerably and is nearly interacting with the bottom-half of the mixing layer at a streamwise distance of $6.2D$. Note

that the peak noise was produced about 30 μs after the second flow image was taken, but the noise event was over 100 μs long, which is the width of the pressure pulse. Therefore, the two images are probably capturing the early part of the noise generating process. The considerable growth and imminent interaction between the two sides of the mixing layer most likely led to the noise production. This type of interaction was observed in areas of intense noise production in several other data sets as well.

The acoustic time trace shown in Fig. 21 has a single large-amplitude event, marked A, that originated from 8.3D ($\tau =$ 0.2950 ms). The front microphone recorded the event with a split peak, while the rear microphone recorded it as a single peak. This will not affect the noise source location technique because it uses the entire pressure pulse to perform the correlation. The sound wave was created about 43 μs after the first flow image was taken and 17 μs before the second flow image was taken ($t_m = 2.2675$ ms). Hence, the noise producing area of the mixing layer was located at 7.8D in the first flow image (Fig. 22) and at 8.5D in the second image (Fig. 23). The noise event was created in the time between the two images. An examination of this area of the jet (the streamwise locations are again marked with white dots) shows that the mixing layer as a whole is being torn into separate sections at this location. It is expected that the intense shear that caused this tearing was the cause of the large-amplitude sound pressure peak that was observed in the acoustic time trace. This is not surprising because the intensity of quadrupole noise, which is the accepted type of noise source for jet mixing noise, is directly related to the strength of the shearing force. Many other data sets also showed that tearing is a noise generation mechanism.

Another noise generation mechanism is shown in the two flow images of Figs. 24 and 25 and the time signature of Fig. 26. The time trace of Fig. 26 has a large negative sound pressure pulse marked A that originated at 7.7D ($\tau = 0.2975$ ms). The noise event was created at about the same time the first flow image was taken ($t_m = 2.2600$ ms). Hence, the noise generating region of the jet was located at 7.7D in Fig. 24 and had convected to about 8.4D in Fig. 25. These areas correspond to a region of very intense interaction between the two sides of the mixing layer. It appears that this interaction led to the production of the large-amplitude sound wave. Similar interactions were also observed in areas of noise production in several other data sets as well.

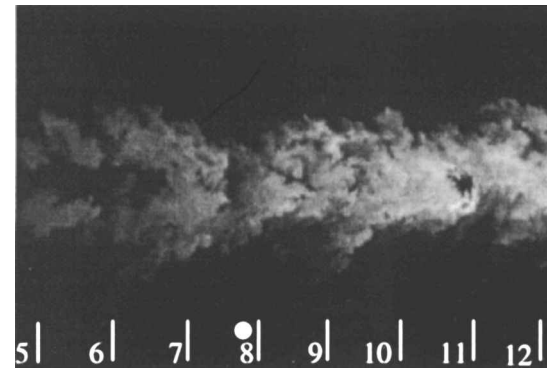

Fig. 22 Simultaneous first flow image for the time trace of Fig. 12; time = 0 μs.

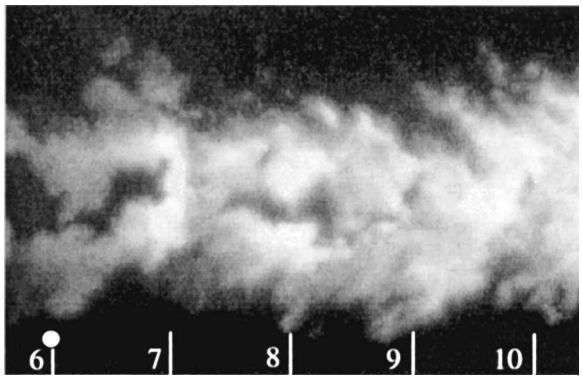

Fig. 20 Simultaneous second flow image for the time trace of Fig. 13; time = 60 μs.

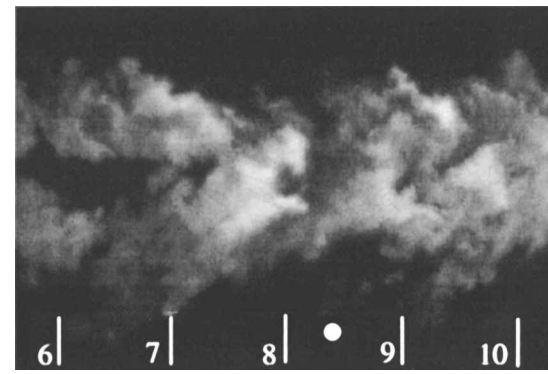

Fig. 23 Simultaneous second flow image for the time trace of Fig. 12; time = 60 μs.

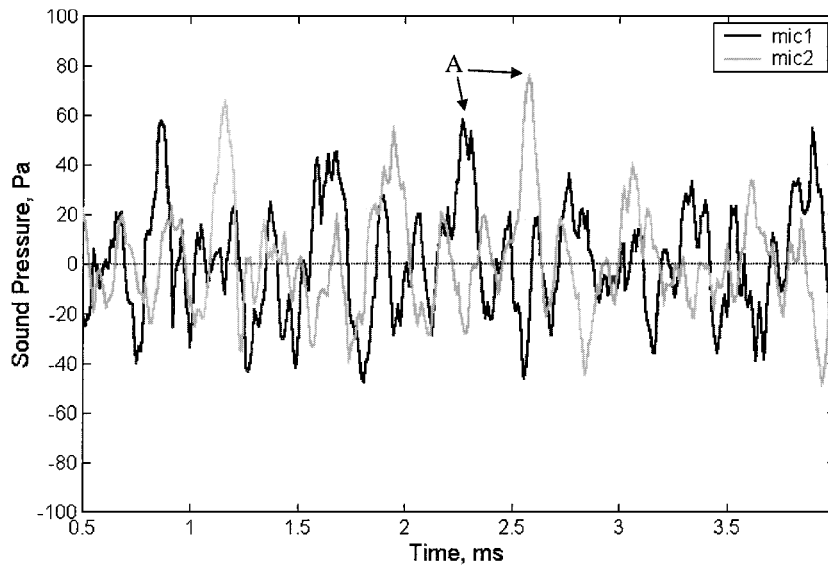

Fig. 21 Time trace of the microphone array data.

The two observed mechanisms of noise generation within the high-Reynolds-number,Mach 1.3 jet discussed were based on many sets of data that were acquired for this work, but only three sets were presented here. The first involves interactions between large structures within the two sides of the mixing layer. This process can be instigated by a single relatively small structure that is growing and interacting with the other side of the mixing layer, as was observed in the data set of Figs. 13, 19, and 20. It could also be caused by two very large structures that extend several jet diameters in the streamwise direction and are in opposite sides of the mixing layer, as was the case in the data set of Figs. 24–26. The second mechanism was the tearing of the mixing layer. In the example shown (the data set of Figs. 21–23), intense noise was generated where shearing had divided the entire jet into two sections. In other data sets, not presented here, it was observed that smaller tears also led to noise production.

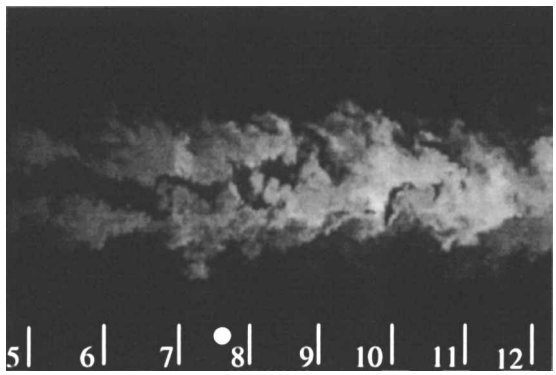

Fig. 24 Simultaneous first flow image for the time trace of Fig. 23; time = 0 μs.

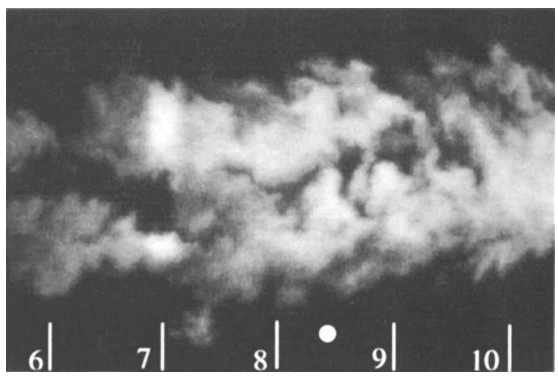

Fig. 25 Simultaneous second flow image for the time trace of Fig. 23; time = 0 μs.

Conclusions

The work presented and discussed represents the initial phase of an ongoing research effort to explore noise sources in high-speed and high-Reynolds-number jets via simultaneous flow and acoustic field measurements. Experiments were conducted to gain knowledge of large-scale turbulence structures and the temporal characteristics of their acoustic far field in a Mach 1.3, high-Reynolds-number, ideally expanded jet. The jet had a potential core length of about $6D$ and a preferential noise emission direction of 30 deg at a preferred frequency of approximately 3 kHz ($St_D = 0.2$). Both symmetric and asymmetric interactions within the structures of the mixing layer of the jet were observed in the instantaneous flow visualization images.

An examination of the far-field sound pressure signal in the time domain and short spectra showed that there are different mechanisms of noise production within the jet. The results showed that large-amplitude sound pressure peaks were interspersed among relatively quiet periods where the jet did not produce any large-amplitude noise. Some of the relatively quiet periods of the jet lasted over 1 ms, which is equivalent to a large structure traveling over 11 jet diameters. Further, the large-amplitude sound events were observed to either come as individual peaks or as a series of oscillating peaks with a fairly well-defined periodicity. These observations lead one to believe that there are distinct events within the jet producing large-amplitude noise emission. Statistical analysis of the temporal acoustic signal showed that the jet is producing the large-amplitude events over 23% of the time, whereas the jet was in relatively quiet modes, enduring at least 0.5 ms, which corresponds to a large structure convecting $5.9D$, 22% of the time. Considering that there is as much as a 10-dB difference between the average spectra of the relatively quiet periods and the periodic peak events of the jet, there is a substantial potential benefit in determining the mechanisms of various noise producing events.

Simultaneous measurements of the acoustic far field by a dual microphone array and double-pulse flow visualizations were acquired to relate the large-amplitude sound events to the large-scale structures of the jet mixing layer. The dual microphone array was used to determine where and when the large-amplitude noise events were produced with respect to the flow images. Using these techniques, the location and mechanism of noise generation was speculated on. Interactions between large structures in the jet mixing layer as well as tearing of the mixing layer seem to be mechanisms of intense noise production.

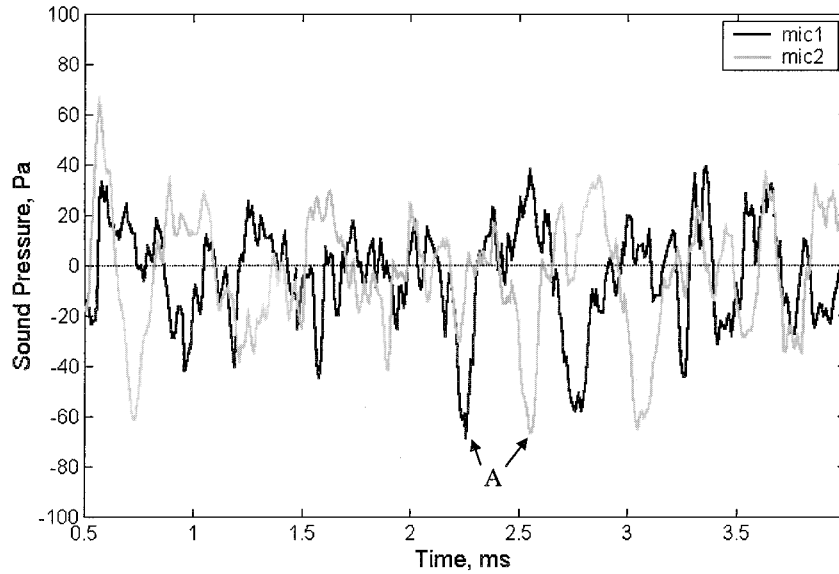

Fig. 26 Time trace of the microphone array data.

These results are very encouraging, but the techniques used in this part of the research were basic and are being improved for the subsequent phase. The microphone array had a fairly large error in source location, which can be reduced significantly. The temporal acoustic analysis technique needs to be augmented with some sort of frequency–time analysis. In many instances, it also proved difficult to identify the interaction between turbulence structures that generated the large-amplitude noise. This is due to the very limited information that can be gathered from double-pulse flow visualizations. Utilizing a real-time flow visualization technique via a pulse burst laser would help to alleviate this problem. Quantitative flow visualization techniques such as planar Doppler velocimetry could also help in interpretation of the nature of the turbulence structures in the jet.

Acknowledgments

This work is supported by the Air Force Office of Scientific Research with Steven Walker as the Technical Monitor. The first author is especially grateful to Jin-Hwa Kim for his aid and guidance in setting up the simultaneous sound/flow visualization experiments. Fruitful discussions with Thomas Barber and Satish Narayanan of the United Technology Research Center, the assistance of Charles Kerechanin for his help in conducting the experiments, and Brian Thurow for editing the manuscript are all greatly appreciated. Furthermore, the authors would like to thank the reviewers of the manuscript for their insight into the jet noise problem and for their suggestions and comments, which improved the quality of the document.

References

[1]Crow, S. C., and Champagne, F. H., "Orderly Structure in Jet Turbulence," *Journal of Fluid Mechanics*, Vol. 48, Pt. 3, 1971, pp. 547–591.

[2]Brown, G. L., and Roshko, A., "On Density Effects and Large Structure in Turbulent Mixing Layers," *Journal of Fluid Mechanics*, Vol. 64, 1974, pp. 715–816.

[3]Hussain, A. K. M. F., "Coherent Structures and Turbulence," *Journal of Fluid Mechanics*, Vol. 173, 1986, pp. 303–356.

[4]Hernan, M. A., and Jimenez, J., "Computer Analysis of a High Speed Film of the Plane Turbulent Mixing Layer," *Journal of Fluid Mechanics*, Vol. 119, 1982, pp. 323–345.

[5]Hussain, A. K. M. F., and Clark, A. R., "On the Coherent Structure of the Axisymmetric Mixing Layer: A Flow-Visualization Study," *Journal of Fluid Mechanics*, Vol. 104, 1981, pp. 263–294.

[6]Bogdanoff, D. W., "Compressibility Effects in Turbulent Shear Layers," *AIAA Journal*, Vol. 21, No. 6, 1983, pp. 926, 927.

[7]Papamoschou, D., and Roshko, A., "The Compressible Turbulent Mixing Layer: An Experimental Study," *Journal of Fluid Mechanics*, Vol. 197, 1988, pp. 453–477.

[8]Elliott, G. S., Samimy, M., and Arnette, S. A., "Study of Compressible Mixing Layers Using Filtered Rayleigh Scattering Based Visualizations," *AIAA Journal*, Vol. 30, No. 10, 1992, pp. 2567–2569.

[9]Clemens, N. T., and Mungal, M. G., "Large Scale Structures and Entrainment in a Supersonic Mixing Layer," *Journal of Fluid Mechanics*, Vol. 284, 1995, pp. 171–216.

[10]Papamoschou, D., and Bunyajitradulya, A., "Evolution of Large Eddies in Compressible Shear Layers," *Physics of Fluids*, Vol. 9, Pt. 3, 1997, pp. 756–765.

[11]Murakami, E., and Papamoschou, D., "Eddy Convection in Coaxial Supersonic Jets," *AIAA Journal*, Vol. 38, No. 4, 2000, pp. 628–635.

[12]Thurow, B., Hileman, J., Samimy, M., and Lempert, W., "An In-Depth Investigation of Large Scale Structure Evolution in a High Speed Axisymmetric Jet," AIAA Paper 2001-0148, Jan. 2001.

[13]Tam, C. K. W., "Jet Noise Generated by Large-Scale Coherent Motion," *Aeroacoustics of Flight Vehicles: Theory and Practice*, Vol. 1, edited by H. H. Hubard, Acoustical Society of America, Woodbury, NY, 1991, pp. 311–390.

[14]Morrison, G. L., and McLaughlin, D. K., "Noise Generation by Instabilities in Low Reynolds Number Supersonic Jets," *Journal of Sound and Vibration*, Vol. 65, No. 2, 1979, pp. 177–191.

[15]Stromberg, J. L., McLaughlin, D. K., and Troutt, T. R., "Flow Field and Acoustic Properties of a Mach Number 0.9 Jet at a Low Reynolds Number," *Journal of Sound and Vibration*, Vol. 72, No. 2, 1980, pp. 159–176.

[16]Simonich, J., Narayanan, S., Barber, T. J., and Nishimura, M., "High Subsonic Jet Experiments Part II: Aeroacoustic Characterization, Noise Reduction and Dimensional Scaling Effects," AIAA Paper 2000-2023, June 2000.

[17]Yu, J. C., and Dosanjh, D. S., "Noise Field of a Supersonic Mach 1.5 Cold Model Jet," *Journal of of the Acoustical Society of America*, Vol. 51, No. 5, Pt. 1, 1972, pp. 1400–1410.

[18]Schaffar, M., "Direct Measurements of the Correlation Between Axial In-Jet Velocity Fluctuations and Far Field Noise near the Axis of a Cold Jet," *Journal of Sound and Vibration*, Vol. 64, No. 1, 1979, pp. 73–83.

[19]Ahuja, K. K., Massey, K. C., and D'Agostino, M. S., "A Simple Technique of Locating Noise Sources of a Jet Under Simulated Forward Motion," AIAA Paper 98-2359, June 1998.

[20]Fisher, M. J., Harper-Bourne, M., and Glegg, S. A. L., "Jet Engine Source Location: The Polar Correlation Technique," *Journal of Sound and Vibration*, Vol. 51, No. 1, 1977, pp. 23–54.

[21]Sarohia, V., and Massier, P. F., "Experimental Results of Large Scale Structures in Jet Flows and Their Relation to Jet Noise Production," AIAA Paper 77-1350, Oct. 1977.

[22]Kibens, V., "Discrete Noise Spectrum Generated by an Acoustically Excited Jet," *AIAA Journal*, Vol. 18, No. 4, 1980, pp. 434–441.

[23]Hussain, A. K. M. F., "Coherent Structures—Reality and Myth," *Physics of Fluids*, Vol. 26, No. 10, 1983, pp. 2816–2850.

[24]Hileman, J., "Identification of Noise Sources in a Mach 1.3 Axisymmetric Jet via Simultaneous Flow and Noise Measurement," M.S. Thesis, Dept. of Mechanical Engineering, Ohio State Univ., Columbus, OH, 2000.

[25]Kerechanin, C. W., Samimy, M., and Kim, J.-H., "Effects of Nozzle Trailing Edge Modifications on Noise Radiation in a Supersonic Rectangular Jet," AIAA Paper 2000-0086, Jan. 2000.

[26]Kerechanin, C., "The Effects of Nozzle Trailing Edge Modifications on the Acoustic Far Field of a Mach 2 Rectangular Jet," M.S. Thesis, Dept. of Mechanical Engineering, Ohio State Univ., Columbus, OH, 2000.

[27]Hileman, J., and Samimy, M., "An Attempt to Identify Noise Generating Turbulent Structures in a High Speed Axisymmetric Jet," AIAA Paper 2000-2020, June 2000.

[28]Hileman, J., Thurow, B., and Samimy, M., "Determination of Noise Sources Within a High-Speed Jet via Simultaneous Acoustic Measurements and Real-Time Flow Visualization," AIAA Paper 2001-0374, Jan. 2001.

[29]Lepicovsky, J., Ahuja, K. K., Brown, W. H., and Burrin, R. H., "Coherent Large-Scale Structures in High Reynolds Number Supersonic Jets," *AIAA Journal*, Vol. 25, No. 11, 1987, pp. 1419–1425.

[30]Thies, A. T., and Tam, C. K. W., "Computation of Turbulent Axisymmetric and Nonaxisymmetric Jet Flows Using the κ–ε Model," *AIAA Journal*, Vol. 34, No. 2, 1996, pp. 309–316.

[31]Seiner, J. M., "Fluid Dynamics and Noise Emission Associated with Supersonic Jets," *Studies in Turbulence*, edited by T. B. Gatski, S. Sarkar, and G. Speziale, Springer-Verlag, New York, 1992, pp. 297–323.

[32]Ffowcs-Williams, J. E., Simson, J., and Virchis, V. J., "'Crackle': An Annoying Component of Jet Noise," *Journal of Fluid Mechanics*, Vol. 71, Pt. 2, 1975, pp. 251–271.

J. P. Gore
Associate Editor